

## Generalized contact process with $n$ absorbing states

Jef Hooyberghs,<sup>1,2</sup> Enrico Carlon,<sup>3</sup> and Carlo Vanderzande<sup>1,4</sup>

<sup>1</sup>*Departement WNI, Limburgs Universitair Centrum, 3590 Diepenbeek, Belgium*

<sup>2</sup>*Aspirant Fonds voor Wetenschappelijk Onderzoek, Vlaanderen, Belgium*

<sup>3</sup>*INFN, Dipartimento di Fisica, Università di Padova, I-35131 Padova, Italy*

<sup>4</sup>*Instituut voor Theoretische Fysica, Celestijnenlaan 200D, 3001 Heverlee, Belgium*

(Received 24 April 2001; published 30 August 2001)

We investigate the critical properties of a one-dimensional stochastic lattice model with  $n$  (permutation symmetric) absorbing states. We analyze the cases with  $n \leq 4$  by means of the nonhermitian density-matrix renormalization group. For  $n=1$  and  $n=2$  we find that the model is, respectively, in the directed percolation and parity conserving universality class, consistent with previous studies. For  $n=3$  and  $n=4$ , the model is in the active phase in the whole parameter space and the critical point is shifted to the limit of one infinite reaction rate. We show that in this limit, the dynamics of the model can be mapped onto that of a zero temperature  $n$ -state Potts model. On the basis of our numerical and analytical results, we conjecture that the model is in the same universality class for all  $n \geq 3$  with exponents  $z = \nu_{\parallel} / \nu_{\perp} = 2$ ,  $\nu_{\perp} = 1$ , and  $\beta = 1$ . These exponents coincide with those of the multispecies (bosonic) branching annihilating random walks. For  $n=3$  we also show that, upon breaking the symmetry to a lower one ( $Z_2$ ), one gets a transition either in the directed percolation, or in the parity conserving class, depending on the choice of parameters.

DOI: 10.1103/PhysRevE.64.0361XX

PACS number(s): 05.70.Ln, 05.70.Jk, 64.60.Ht, 02.60.Dc

### I. INTRODUCTION

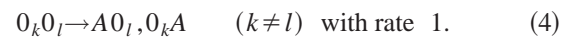
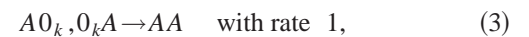
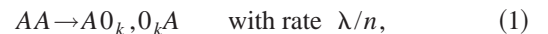
The study of systems out of thermal equilibrium has attracted great attention in recent years. As their equilibrium counterparts, these systems may display continuous phase transitions characterized by a set of critical exponents [1]. In particular, much interest exists in transitions from a fluctuating active state towards an absorbing state, i.e., a configuration where the dynamics is frozen.

A prototype of a one dimensional (1D) lattice model with a transition into an absorbing state is the contact process [1,2] in which each lattice site can be either empty (0) or occupied by a particle (A) with the reactions  $A \rightarrow 2A$ ,  $A \rightarrow 0$ . Depending on the relative rates of these processes, the stationary state is empty (when  $A \rightarrow 0$  dominates), or is occupied by a finite density of particles (if the reaction  $A \rightarrow 2A$  dominates). The contact process therefore displays a nonequilibrium phase transition that is known to belong to the directed percolation (DP) universality class. The empty lattice (00...0) is the absorbing state.

A wide range of models with transitions into absorbing states was found to belong to the DP universality class. As typical examples, we quote the branching-annihilating random walks (BARW) with an odd number of offsprings [3], the Domany-Kinzel model [4], and the pair contact process [5]. The DP class therefore appears to be extremely robust and quite common, but it is certainly not the only possible one.

Another universality class that has by now been firmly established is the so-called parity conserving (PC) class [1]. A prototype model in this class is the BARW with an even number of offsprings [6] in which particles can diffuse and undergo the reactions  $2A \rightarrow 0$ ,  $A \rightarrow (m+1)A$ , with  $m$  an even integer. In that model, the particle conservation modulo two is believed to be the reason for the system to show non-DP critical behavior. More recently, it became clear that the par-

ity conservation, at least at the microscopic level, is not a necessary condition for a PC transition to occur [7,8]. Hinrichsen [8] provided an example of this by introducing a one-dimensional model where each lattice site can be occupied by, at most, one particle or can be in any of  $n$  inactive states ( $0_1, 0_2, \dots, 0_n$ ). The reactions are:



We refer to the model defined by the reactions (1–4) as to the generalized contact process (GCP). The original contact process [2], corresponds to the case  $n=1$ , in which the reaction (4) is obviously absent. Notice that the reaction (4) in the case  $n \geq 2$  ensures that configurations as  $(0_i 0_i \dots 0_i 0_i 0_j 0_j \dots 0_j 0_j)$ , with  $i \neq j$  are not absorbing. Such configurations do evolve in time until the different domains coarsen and one of the  $n$  absorbing states ( $0_1 0_1 \dots 0_1$ ), ( $0_2 0_2 \dots 0_2$ )  $\dots$  ( $0_n 0_n \dots 0_n$ ) is reached.

For the GCP with  $n=2$ , it was found from simulations [8] that the transition falls in the PC class if  $\mu_1 = \mu_2$ , while if the symmetry between the two absorbing states was broken, ( $\mu_1 \neq \mu_2$ ) a DP transition was recovered [8].

One aim of this paper is to investigate the case  $n \geq 3$ , which has not been studied so far. Our results are obtained by a numerical investigation based on density-matrix renormalization group (DMRG) techniques [9] for the case  $n=3$  and  $n=4$  and an exact solution in the limit  $\mu \rightarrow \infty$ . On the basis of these results, we are led to conjecture that for  $n$

$\geq 3$  the model is always in the same universality class, which coincides with that of multispecies branching and annihilating random walks [10].

There are several reasons that make the GCP interesting. First, it contains the two major universality classes for transitions into absorbing states, namely DP ( $n=1$ ) and PC ( $n=2$ ). Second, for  $n>1$ , it is interesting to study the effect of breaking the permutational symmetry of the model, and for  $n>2$ , the symmetry can be broken in different ways (see below). Finally, it is also interesting to investigate the performance of the DMRG algorithm for a system with several absorbing configurations and with several states per site, a situation that is definitely more complicated than what was considered so far [11,12]. We recall that the application of the DMRG to nonequilibrium processes is rather recent and its power/limitations have not been fully investigated yet, therefore, the GCP represents another important testing ground for this purpose.

This paper is organized as follows: in Sec. II, we present the numerical results for the cases  $n=1,2,3$ , and 4. In Sec. III, we show that in the limit  $\mu \rightarrow \infty$  the dynamics of the model can be mapped onto that of the zero temperature  $n$ -state Potts model, which allows the determination of one critical exponent. Next, we present in Sec. IV a conjecture for the critical behavior of the model for  $n \geq 3$  based on the numerical and exact results. Finally, in Sec. V, we analyze the effect of breaking the symmetry in the  $n=3$  case, while Sec. VI concludes the paper.

## II. DMRG STUDY OF THE MODEL

As a starting point for our analysis, we use the quantum form of the master equation [13,14] to describe the evolution of the stochastic processes in continuous time:

$$\frac{d|P(t)\rangle}{dt} = -H|P(t)\rangle, \quad (5)$$

where  $|P(t)\rangle$  is a state vector whose elements are the probabilities of finding the system in a certain configuration, and the entries of the matrix  $H$  are the transition probabilities per unit of time between different configurations. As in quantum mechanics, we will call  $H$  the Hamiltonian of the system. However, in the most general case, as in the GCP, the matrix  $H$  is nonhermitian, therefore, one should distinguish between right and left eigenvectors, which are now not related by transposition. As a second consequence, the eigenvalues could be complex, but  $H$  always has at least one eigenvalue that is zero, and the real part of the nonvanishing eigenvalues is strictly positive. Since we are interested in the stationary behavior of the system and the relaxation towards it, we will determine the low-lying spectrum of the Hamiltonian, i.e., the part of the spectrum with the smallest real part. In Secs. II–IV we will consider the system to be symmetric in the ground states:  $\mu_1 = \mu_2 = \dots = \mu$ .

First of all, the conservation of probability always ensures the existence of a trivial left eigenvector with zero eigenvalue  $\langle 0 | \equiv \sum_{\sigma} \langle \sigma |$ , where the sum is extended over all possible configurations  $\langle \sigma |$ . Besides this left ground state, the

GCP has  $n$  trivial right ground states: the  $n$  absorbing configurations  $|\psi_k^0\rangle \equiv |0_k 0_k, \dots, 0_k\rangle$ , with  $k=1,2,\dots,n$ . To study the rest of the low-lying spectrum, we apply the DMRG in combination with finite-size scaling. The DMRG is an iterative algorithm through which one constructs approximate eigenvalues and eigenvectors of  $H$  for long chains. At each iteration, the lattice size is increased and the configurational space is truncated efficiently, so that one considers, instead of the exact operator  $H$ , effective matrices of reduced dimensions, which can be handled numerically. The accuracy obtained for the dominant eigenvalues and eigenvectors is often very good. Although originally invented for hermitian problems, the DMRG also works in nonhermitian cases, as it has been shown in several examples [11,12].

### A. The cases $n=1$ and $n=2$

For  $n>1$ , the GCP has more than one absorbing state, and therefore, more than two states per site. This, together with the fact that the Hamiltonian is nonhermitian, makes a DMRG study of the model technically difficult. Consequently, it is of great importance to have a way to check the results of our method. Until now, the GCP has only been studied by means of Monte Carlo simulations, for  $n=1,2$  [8]. Therefore, this section is restricted to these two cases. We will explain how we applied the DMRG, give some details on the finite size scaling for  $n=2$ , and compare our results with [8].

A first quantity that can be calculated by the DMRG is the gap  $\Gamma$  between (the real part of) the eigenvalue of the first excited state of the Hamiltonian  $H$  and the absorbing ground states  $|\psi_k^0\rangle$ .  $\Gamma$  is the inverse relaxation time and enables us to determine the critical region and the dynamical critical exponent  $z = \nu_{\parallel} / \nu_{\perp}$ . A direct implementation of the DMRG is however very unpractical since for  $n>1$  we have a degenerate ground state, and the DMRG is known to work best for gapped systems. We alleviated this problem by adding, at the two boundary sites, the following reactions:

$$0_k \rightarrow 0_1 \quad (k \neq 1) \quad \text{with rate } p. \quad (6)$$

(Recall that it is customary to use open boundary conditions in DMRG [9].) With Eq. (6), only  $|\psi_1^0\rangle$  is left as a ground state. The bulk critical behavior is however expected to be unchanged. Next, we performed the transformation [15]:

$$H'(\Delta) \equiv H + \Delta |\psi_1^0\rangle \langle 0|, \quad (7)$$

with  $\Delta > 0$  and where  $H$  is constructed from the reactions (1–4) and Eq. (6).  $H'$  is no longer a stochastic Hamiltonian, the zero eigenvalue is shifted to  $\Delta$ , but the rest of its spectrum is exactly the same as that of  $H$ . This can easily be checked by looking at the eigenvalues of the left eigenvectors that are the same for both matrices. Therefore, the calculation of the gap of the original Hamiltonian with an  $n$ -times degenerate ground state is reduced to the calculation of the lowest eigenvalue of  $H'$  (obviously provided  $\Delta$  is bigger than the gap of  $H$ ). This strategy could be generalized to other systems with several absorbing states, provided one

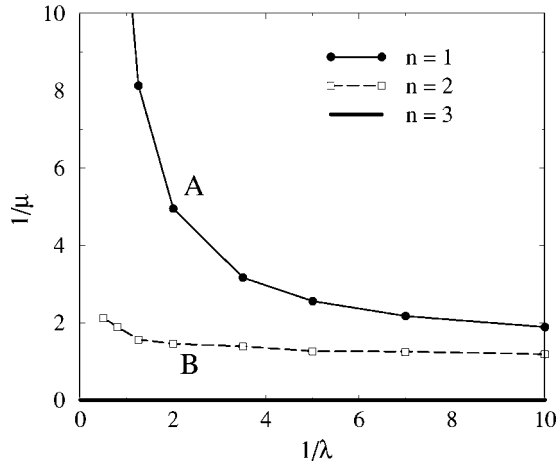


FIG. 1. Phase diagram of the generalized contact process for  $\mu_1 = \mu_2 = \dots = \mu_n = \mu$ , as obtained by nonhermitian DMRG techniques, for  $n=1$  (filled circles),  $n=2$  (empty squares), and  $n=3$  (thick solid line). For  $n=1$  and  $n=2$ , the region above the curves is the active phase, while the region below is inactive. In the limit  $\lambda \rightarrow \infty$ , the critical line for  $n=2$  approaches a finite value of  $\mu$ , while that for  $n=1$  diverges towards  $\mu \rightarrow 0$ . In the other limit  $\lambda \rightarrow 0$ , both lines merge into a common special point (see Ref. [8]). For  $n=3$ , the model is active in the whole parameter space except along the critical line  $1/\mu=0$ .

finds an appropriate boundary reaction that “eliminates” zero eigenstates, as done by Eq. (6) for the GCP.

Before turning to the finite-size analysis of the calculated gap, let us first present the phase diagram for  $n=1$  and  $n=2$ . Figure 1 shows these diagrams, obtained by the DMRG method and standard finite-size scaling techniques. The region above the lines denotes the active state, where the system has a finite stationary density of particles, while below these lines, the stationary density is zero and the system is in one of the absorbing states. We find (see below) that the critical exponents are the same all along the critical line and are those of the DP and PC universality class for  $n=1$  and  $n=2$ , respectively. We notice that the active region increases from  $n=1$  to  $n=2$ . The location of the critical lines agrees well with Monte Carlo simulations by Hinrichsen [8].

It is worth while at this point to present in some more detail, the finite-size scaling analysis employed for  $n=2$ , in order to clarify the differences with the higher  $n$  case. For each choice of the rates  $(\lambda, \mu)$  we can calculate the gap  $\Gamma_L$  of the matrix  $H$  for a system of length  $L$ . This gap equals the lowest eigenvalue of  $H'$  defined in Eq. (7). As a function of  $L$ ,  $\Gamma_L$  has a different scaling behavior in the three regions of the phase diagram. In the active phase, the gap should scale as  $\Gamma_L \sim \exp(-aL)$ , since asymptotically in  $L$ , the absorbing states are degenerate with a state having a finite density of particles. At the critical line we have  $\Gamma_L \sim L^{-z}$ , with  $z = \nu_{\parallel}/\nu_{\perp}$  the dynamical exponent. For  $n=2$  the system is in the PC universality class and the whole inactive phase is known to be algebraic: the gap decays as  $\Gamma_L \sim L^{-2}$ . Notice that the latter behavior is different in DP models where the gap is finite, i.e.,  $\Gamma_L \sim \Gamma_0 > 0$ , in the inactive phase.

The finite-size scaling behavior of  $\Gamma_L$  can best be monitored by plotting the discrete logarithmic derivative of the

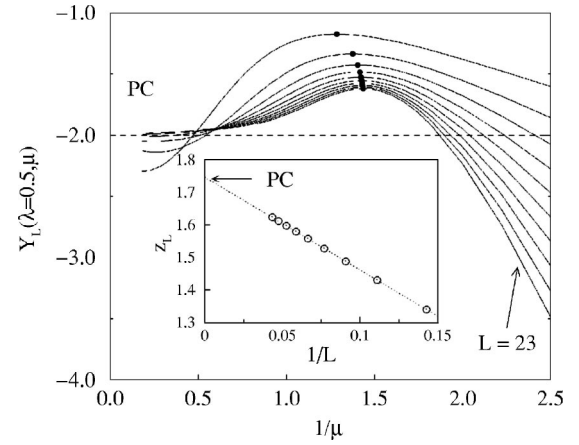


FIG. 2. Plot of  $Y_L$  for the GCP with  $n=2$  as function of  $\mu$  and for  $\lambda=0.5$ . Inset: plot of  $z_L$  as a function of the inverse system length  $1/L$ . The horizontal lines indicate the values two and the known value of the exponent  $z$  for the PC universality class ( $z = 1.74$ ).

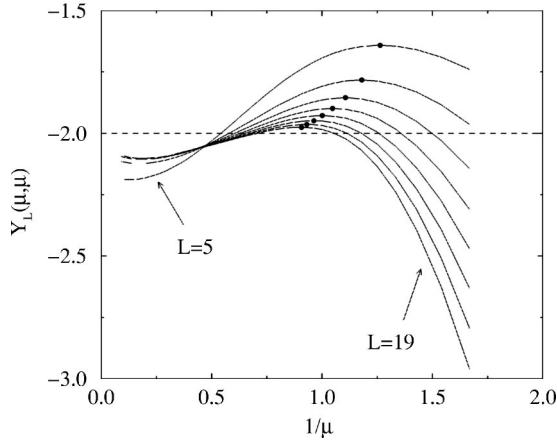
gap:  $Y_L \equiv \ln(\Gamma_{L+1}/\Gamma_{L-1})/\ln[(L+1)/(L-1)]$ . In the active phase, the scaling form  $\Gamma_L \sim \exp(-aL)$  implies  $Y_L \sim -aL$  (with  $a$  a positive constant), while  $Y_L \sim -z$  at the critical line.

Figure 2 shows a plot of  $Y_L$  for  $n=2$ ,  $\lambda=0.5$  as a function of the parameter  $\mu$  for  $L=5, 7, \dots, 23$  (in the present case, the calculation of the gap was extended up to  $L=24$ ). In the right part of the figure, one distinguishes the scaling for the active phase, while in the left part (large  $\mu$ ), one sees that  $Y_L$  flattens out and approaches the value of  $-2$ , as expected for the algebraic inactive phase of PC models. The maxima of  $Y_L$ , marked with a filled circle in Fig. 2, identify the boundary between the active and inactive phase and can be used as critical point estimates. From an  $L \rightarrow \infty$  extrapolation we find  $\mu_c = 0.69(1)$  for our choice of  $\lambda = 0.5$ , which determines point  $B$  of the critical line in Fig. 1. In the inset of Fig. 2 we plot  $z_L = -\max_{\mu} Y_L(\mu, \lambda=0.5)$ , as a function of  $1/L$ . Extrapolating  $z_L$  in the limit  $L \rightarrow \infty$  we find  $z_L \rightarrow 1.747$ , in accurate agreement with the corresponding exponent known for the PC class  $z = \nu_{\parallel}/\nu_{\perp} = 1.74(1)$  [16].

In this way, the DMRG enables us to determine the critical region and the exponent  $z$ . As we will show in the following subsection, using different boundary conditions we can also find estimates for other exponents. In Table I, we show our estimates of the critical exponents  $z$  and  $\beta/\nu_{\perp}$ , in the points  $A$  and  $B$  of Fig. 1. We recover the exponents of DP and PC as expected for  $n=1$  and  $n=2$ , respectively, indicating that the DMRG is performing well.

TABLE I. Estimates for the critical exponents  $z = \nu_{\parallel}/\nu_{\perp}$  and  $\beta/\nu_{\perp}$  calculated for  $n=1$  and 2 absorbing states. We recall that for DP  $z = 1.5806$ ,  $\beta/\nu_{\perp} = 0.25$  and for PC  $z = 1.75$ ,  $\beta/\nu_{\perp} = 0.50$ .

$n$	$\lambda$	$\mu_c$	$z = \nu_{\parallel}/\nu_{\perp}$	$\beta/\nu_{\perp}$
1	0.5	0.20(1)	1.575(5)	0.255(5)
2	0.5	0.69(1)	1.747(5)	0.49(1)


 FIG. 3. Plot of  $Y_L$  for the GCP with  $n=3$  along the line  $\lambda = \mu$ .

### B. The case $n=3$

Since the results of the DMRG are consistent with the Monte Carlo results for  $n=1$  and  $n=2$ , we can confidently use it to study also the case  $n=3$ . Again we start by an analysis of the gap: in Fig. 3 we plot the quantity  $Y_L$  along the line  $\lambda = \mu$  for  $L=7, 9, \dots, 19$ . As for  $n=2$ , we find clear evidence of an active phase for small  $\mu$  where  $Y_L \sim -aL$ . However, when we want to determine the critical point by localizing the maxima, we find that upon increasing  $L$ , the maxima shift towards larger values of  $\mu$ . In the limit  $L \rightarrow \infty$ , we find  $\mu_{\max} \rightarrow \infty$ , indicating that the system is always active and that the critical point is shifted to  $1/\mu = 0$ . This numerical evidence, together with the arguments presented in the next section, lead us to expect that the model is critical only if  $1/\mu = 0$ , as indicated in Fig. 1. The estimate of the exponent  $z$  at  $\lambda = \mu \rightarrow \infty$  yields  $z = 2.00(3)$ . In the next section, we will give an analytical treatment of the case  $1/\mu = 0$  confirming this value of  $z$ .

To get access to more critical exponents, we introduce different boundary conditions. We replace Eq. (6) with

$$0_k \rightarrow A \quad \text{with rate } p' \quad \forall k, \quad (8)$$

through which particles are continuously injected at the boundary sites. Now the states  $|\psi_k^0\rangle$  are no longer absorbing configurations, and the spectrum of the Hamiltonian is non-degenerate. There is a unique right eigenvector  $|\phi_0\rangle$ , which for finite system lengths always has a finite density of particles. In the active phase, the gap  $\Gamma'_L$  is no longer asymptotically degenerate, as in the previous case, but it remains finite, indicating that the system relaxes exponentially fast towards  $|\phi_0\rangle$ . Summarizing, if we consider the model defined by the reactions (1)–(4) and the boundary term (8) we have a gap behaving as  $\lim_{L \rightarrow \infty} \Gamma'_L = \Gamma_0 > 0$  in the active phase, while as before  $\Gamma'_L \sim L^{-z}$  at the critical point. This means we can use  $\Gamma'_L$  itself to discriminate between the active and critical domains.

Figure 4 shows a plot of the gap  $\Gamma'_L$  along the line  $\lambda = \mu$ . When we extrapolate  $L \rightarrow \infty$ , the gap remains finite for every value of  $\mu$ , i.e., we find again that the system is active throughout the whole parameter space.

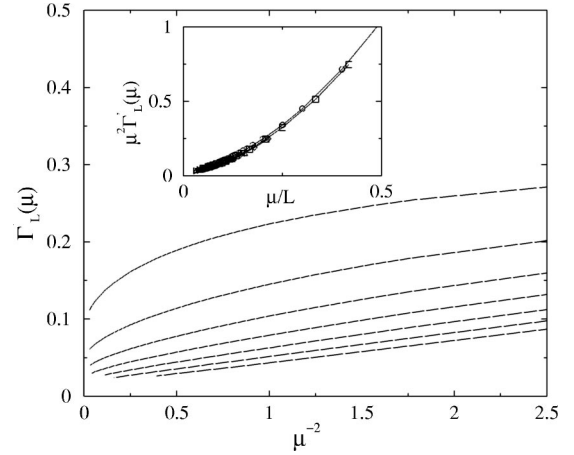


FIG. 4. Plot of the gap  $\Gamma'_L(\mu)$ , calculated along the line  $\lambda = \mu$  [with  $p' = \mu$  in reaction (8)] as function of  $\mu^{-2}$  for systems of lengths  $L=6, 8, \dots, 18$ . Inset: scaling collapse of  $\mu^{\nu_{\parallel}} \Gamma'_L(\mu)$ , plotted as function of  $\mu L^{-1/\nu_{\perp}}$  for  $L=10, 12, 14, 16, \text{ and } 18$  and where we used  $\nu_{\parallel} = 2$  and  $\nu_{\perp} = 1$ .

These data also give the possibility to estimate the correlation length exponent along the time direction:  $\nu_{\parallel}$ . Finite-size scaling around the critical point  $1/\mu = 0$  gives us the following scaling relation:

$$\Gamma'_L(\lambda = \mu) = \mu^{-\nu_{\parallel}} f(\mu L^{-z/\nu_{\parallel}}). \quad (9)$$

For  $\mu$  fixed and  $L \rightarrow \infty$ ,  $\Gamma'_L$  remains finite, so the scaling function should behave like  $\lim_{x \rightarrow 0^+} f(x) = f_0$ . As a consequence in the thermodynamic limit  $L \rightarrow \infty$ , the gap should vanish at the critical point as  $\Gamma'_L \sim \mu^{-\nu_{\parallel}}$ . The linear behavior of the gap in Fig. 4, when plotted as a function of  $\mu^{-2}$ , already indicates that  $\nu_{\parallel} = 2$  and this results is also consistent with the scaling collapse reported in the inset, where we took  $\nu_{\parallel} = 2$  and  $z = 2$ .

Finally, using the same boundary term (8) it is also possible to compute the critical exponent  $\beta$  that describes the behavior of the particle density near the critical point. With the boundary condition (8), the stationary state of any finite system has a nonzero density of particles. We calculated, in particular, the average density of particles in the central site of the chain that we will denote as  $\rho_L(\lambda, \mu)$ . This quantity, calculated along the line  $\lambda = \mu$ , is shown in Fig. 5 for chains of various lengths (up to  $L=24$ ) and plotted as function of  $1/\mu$ . For large  $\mu$  and  $\lambda$  ( $\mu \geq 2$ ), the DMRG does not perform so well and we had to restrict the calculation to  $L=14$ .

As seen in the figure in the limit  $L \rightarrow \infty$ , the stationary particle density vanishes only for  $\mu \rightarrow \infty$ , again indicating that the system is always active for any finite  $\mu$ . For large  $\mu$ , the order parameter is expected to decay as  $\rho \sim \mu^{-\beta}$ , therefore the quantity

$$\beta_{\text{eff}}(\mu, L) = - \frac{d \ln \rho_L(\lambda = \mu)}{d \ln \mu} \quad (10)$$

converges to  $\beta$  for  $L \rightarrow \infty$  and  $\mu \rightarrow \infty$ . The inset of Fig. 5 shows a plot of  $\beta_{\text{eff}}$  as a function of  $1/\mu$  for chains of various



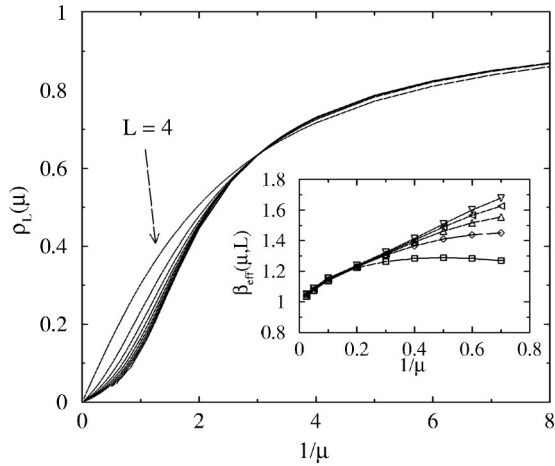


FIG. 5. Plot of the stationary particle density  $\rho$  for the model with  $n=3$  absorbing states along the line  $\mu=\lambda$  for various system sizes ( $L=4, 6, \dots, 24$ ). For large  $\mu$ , the calculation has been limited to  $L=14$ . Inset: plot of the effective exponent  $\beta$  as function of  $1/\mu$  for  $L=6$  (lower curve) up to  $L=14$  (upper curve).

system lengths. The extrapolated result for  $L=12$  and  $L=14$  is  $\beta=1.00(1)$ . (See Fig 5.)

In summary, we found that for  $n=3$ , the system is always active, except for  $1/\mu=0$  where it is critical and we have exponents consistent with  $z=2$ ,  $\nu_{\parallel}=2$ ,  $\beta=1$ .

### C. The case $n=4$

To conclude our numerical calculations for the case of symmetrical ground states, we studied the system with four inactive states per site. Here, we restricted ourselves to a calculation of the density  $\rho_L(\lambda, \mu)$  with boundary condition (8). Our results are shown in Fig. 6.

From these data we find, as was the case for  $n=3$ , that the system is active for any finite value of  $\mu$ , and that the critical exponent  $\beta=0.98(4)$ .

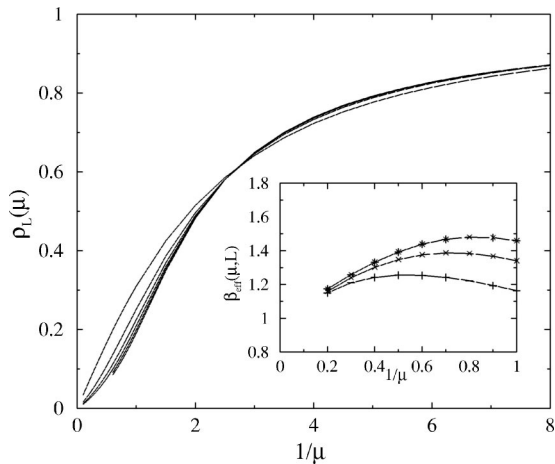
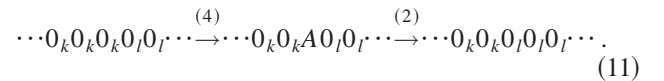


FIG. 6. Plot of the stationary particle density  $\rho$  for the model with  $n=4$  absorbing states along the line  $\mu=\lambda$  for various system sizes ( $L=4, 6, \dots, 14$ ). For large  $\mu$ , the calculation has been extended up to  $L=10$ . Inset: plot of the effective exponent  $\beta$  as function of  $1/\mu$  for  $L=6$  (lower curve) up to  $L=10$  (upper curve).

### III. FAST RATE EXPANSION FOR $\mu$ OR $\lambda \rightarrow \infty$

In this section, we show how the dynamics of the model can be simplified in the limit where one of the rates of the decay processes (1) or (2) goes to infinity. For  $\mu \rightarrow \infty$ , the resulting effective dynamics coincides with that of a zero temperature  $n$ -state Potts model. This leads to a determination of the exponent  $z$ .

Intuitively, the argument goes as follows. For  $\mu \rightarrow \infty$ , all particles in the system will disappear very quickly, and in any finite system one will soon be in a configuration containing only the  $n$  empty sites  $0_1, 0_2, \dots, 0_n$ . Particles will then be created at the boundaries separating inactive domains by Eq. (4), but again they will disappear immediately by reaction (2). Hence, when looked at the time scale of the slow processes (3) and (4) the dynamics can be limited to the set of configurations that contain only empty sites. [In this limit, the creation of two particles on nearest-neighbor sites occurs with even smaller probability and the effect of Eq. (1) can therefore be neglected]. As an example consider:



The whole process consists of moving the domain wall one unit to the left with rate (on the time scale of the slow process) equal to  $1/2$ . Going in this way through all possibilities one can derive an effective dynamics on the slow time scale, which turns out to involve diffusion, annihilation and coagulation of domain walls.

The above heuristic reasoning can be made mathematically rigorous using a fast rate expansion introduced in [14]. We therefore write  $H$  as

$$H = H_0 + \mu H_1, \quad (12)$$

where  $H_0$  contains the reactions (1), (3), and (4) while  $H_1$  contains only the reactions (2). In the limit  $\mu \rightarrow \infty$ , it is appropriate to apply the Schwinger-Dyson formula to the operator  $e^{-Ht}$  that appears in the formal solution of the master equation (5). One has

$$e^{-(H_0 + \mu H_1)t} = e^{-\mu H_1 t} \left[ 1 - \int_0^t d\tau_1 H_0(\tau_1) + \int_0^t d\tau_1 \int_0^{\tau_1} d\tau_2 H_0(\tau_1) H_0(\tau_2) + \dots \right], \quad (13)$$

where

$$H_0(\tau) = e^{\mu H_1 \tau} H_0 e^{-\mu H_1 \tau}. \quad (14)$$

Using this expansion it can be shown [14] that for  $\mu \rightarrow \infty$  the time evolution operator  $e^{-Ht}$  becomes

$$\lim_{\mu \rightarrow \infty} e^{-(H_0 + \mu H_1)t} = e^{-\tilde{H}_0 t} T^*, \quad (15)$$

where

$$\tilde{H}_0 = T^* H_0 T^* \quad (16)$$

and  $T^*$  is the projector on the ground states of  $H_1$ , i.e.,

$$T^* = \lim_{t \rightarrow \infty} e^{-H_1 t}. \quad (17)$$

Equation (15) shows that for  $\mu \rightarrow \infty$ , the generator of the effective dynamics is  $\tilde{H}_0$  that is nothing but  $H_0$  projected onto the ground states of  $H_1$ . In the GCP, the ground states of  $H_1$  for a chain of length  $L$  are the  $n^L$  configurations without particles and  $\tilde{H}_0$  is then the effective Hamiltonian of the slow processes projected in this reduced space. This is the mathematical description of the physical arguments given in the beginning of this section. If one works out the matrix elements of  $\tilde{H}_0$  (see the Appendix) one obtains that the following processes can occur with the indicated rates:

$$0_k 0_l 0_k \rightarrow 0_k 0_k 0_l \quad \text{rate } 2, \quad (18)$$

$$\begin{aligned} 0_k 0_l 0_l &\rightarrow 0_k 0_k 0_l & \text{rate } 1/2, \\ &\rightarrow 0_k 0_l 0_l & \text{rate } 1/2, \end{aligned} \quad (19)$$

$$\begin{aligned} 0_k 0_l 0_m &\rightarrow 0_k 0_k 0_m & \text{rate } 1, \\ &\rightarrow 0_k 0_m 0_m & \text{rate } 1. \end{aligned} \quad (20)$$

It is now useful to interpret the  $n$  empty states as the possible spin values of an  $n$ -state Potts model. In this language, the processes (18–20) can be summarized as follows: the central spin assumes the value of one of its neighbor spins with equal probability. The dynamics of our model in the limit  $\mu \rightarrow \infty$  is therefore consistent with the requirements of detailed balance for an  $n$ -state Potts model at zero temperature. It is generally expected that if such a dynamics includes a domain-wall diffusion, that then it is critical with a dynamic exponent  $z=2$  [17], independently of  $n$ . In fact, the exponent  $z=2$  can be derived exactly for the case that the rate of the process (18) equals one, and those of the processes in Eq. (20) equal  $1/2$  [18]. Hence, it is quite possible that also for our model,  $z=2$  exactly. For  $n=2$ , we thus recover the known dynamical exponent  $z=2$  in the inactive phase of a model with a PC transition. For  $n \geq 3$  our numerical data strongly suggest that for  $\mu \rightarrow \infty$ , the GCP is critical, and hence, the exponent  $z=2$  must correspond to the dynamical exponent at criticality for these models. This estimate is indeed consistent with the value that was determined numerically for  $n=3$  in the previous section.

The result that numerically the exponent  $\beta$  is the same for  $n=3$  and  $n=4$ , combined with the fact that  $z=2$  if  $n \geq 3$  leads us to conjecture that for all  $n \geq 3$ , the critical exponents are the same, i.e.,  $\beta=1$ ,  $z=2$ , and  $\nu_{\parallel}=2$ . In the next section we will give further arguments that support this conjecture.

It is also possible to study the effective dynamics of the GCP for  $\lambda \rightarrow \infty$ . In this limit, the dynamics of the model when considered on the time scale of the slow processes (2)–(4), will be restricted to the space of configurations without particle pairs. Each particle present in the system then separates two domains of empty sites. Therefore, particles

can be labeled by two indices and in this way they can be divided into classes. We will denote by  $A_{ij}$  a particle  $A$  that separates an  $0_i$  domain on its left side from an  $0_j$  domain on its right side. In the limit  $\lambda \rightarrow \infty$ , it is useful to look at the dynamics of these particles. When  $n=1$ , there is only one type of particle, and from a determination of the effective Hamiltonian  $\tilde{H}_0$  (see the Appendix) we find that this particle can diffuse, and undergo the reactions  $2A \rightarrow A$  and  $A \rightarrow 0$ . Since there are no processes that create particles, we arrive at the conclusion that independently of  $\mu$ , the GCP with  $n=1$  must always be in the inactive state when  $\lambda \rightarrow \infty$ . This is in agreement with our numerical results (see Fig. 1).

For  $n > 1$ , the situation is less clear. Now there are processes that both destroy and create particles present in the effective dynamics (see the Appendix). It is therefore, in principle, possible to have both an active and an inactive phase, depending on the value of  $\mu$ . At this moment, we can draw no firm conclusions for the form of the phase diagram when  $\lambda \rightarrow \infty$ . On the basis of our numerical work and on the basis of our results for  $\mu \rightarrow \infty$ , we believe that the model is probably always active along that line, at least when  $n > 2$ .

#### IV. RELATION WITH BRANCHING AND ANNIHILATING WALKS

In his paper, Hinrichsen [8] gave an heuristic argument that relates the GCP for  $n=2$  to the BARW with two offsprings, thus explaining the PC universality found numerically. This argument works as follows: indicating with  $X_{ij}$  the domain wall between two configurations  $0_i$  and  $0_j$  he considered an effective dynamics for the variables  $X_{ij}$ . As seen in the previous section such representation of the original model becomes exact either in the limit  $\lambda \rightarrow \infty$  and then  $X_{ij}$  coincides with the particle  $A_{ij}$ , or in the limit  $\mu \rightarrow \infty$  where  $X_{ij}$  coincides with the bond variable  $0_i 0_j$ . For finite values of these parameters one can still apply this reasoning at a coarse-grained level. In this case,  $X_{ij}$  is not a sharp domain wall, but an object with a fluctuating thickness. Hinrichsen argued that in this coarse-grained representation the most likely reactions for  $n=2$  are

$$\begin{aligned} \text{(a)} \quad X_{ij} &\rightarrow X_{ij} X_{ji} X_{ij} & \text{(b)} \quad X_{ij} X_{ji} &\rightarrow 0, \end{aligned} \quad (21)$$

(for  $n=2$ , one has obviously  $i=1$ ,  $j=2$  or viceversa). An example of such reactions is shown in Figs. 7(a) and (b). Notice that the reactions (a) and (b) given in Eq. (21) are those for a branching-annihilating random walk (BARW) with two offsprings, which suggests indeed, as found numerically that the universality class is PC.

These arguments can be extended to the case  $n > 2$ , where there is still the possibility of having reactions of type (a) and (b), but also reactions involving three different domains ( $i \neq j$ ,  $i \neq k$ , and  $j \neq k$ ):

$$\begin{aligned} \text{(c)} \quad X_{ij} &\rightarrow X_{ik} X_{kj} & \text{(d)} \quad X_{ik} X_{kj} &\rightarrow X_{ij}. \end{aligned} \quad (22)$$

When  $n > 2$  there are actually  $n(n-1)/2$  domain walls, and the model described by reactions (21) and (22) is now a

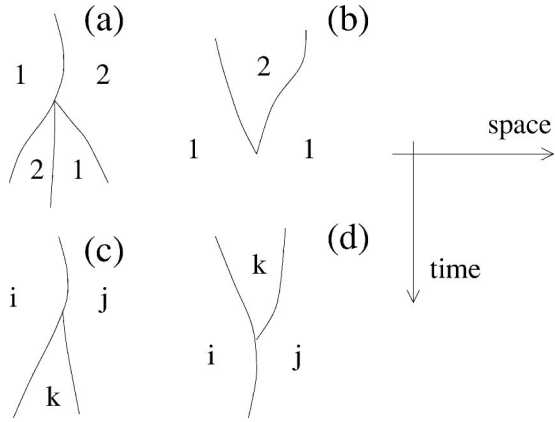
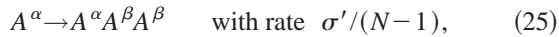


FIG. 7. Possible reactions in the coarse-grained representation of the GCP for  $n=2$  (a)–(b) and  $n>2$  (a)–(d).

BARW with more than one type of particles. To our knowledge, this type of model has not been studied yet, but we expect it to be in the same universality class as the GCP with  $n>2$ , i.e., always in an active state except when the rates for the processes (a) and (c) are zero, and with exponents  $z=2$ ,  $\beta=1$  and  $\nu_{\parallel}=2$ .

There is a BARW with more than one type of particles that has attracted some attention recently. The model was introduced by Cardy and Täuber [10], who considered a system with  $N$  different particles  $A^{\alpha}$ , where  $\alpha=1,2,\dots,N$ , which diffuse and undergo the reactions:



where, in the last reaction, it is understood that  $\alpha \neq \beta$ . The *bosonic* version of this model has precisely the same exponents we determined for the GCP with  $n>2$  [10]. Notice that the coarse-grained representation of the GCP as defined by the reactions in Fig. 7 and the model defined by the reactions (23), (24), (25) do not actually coincide. While there is an obvious correspondence between (23), (24), with (b), (a) of Fig. 7, the reaction (25) does not have any obvious counterpart. It is not *a priori* clear, therefore, that the two models are in the same universality class. The coincidence of the critical exponents therefore suggests that one could replace Eq. (25) with other reactions, as for instance  $A^{\alpha} \rightarrow A^{\gamma}A^{\delta}$ , without changing the universality class. To our knowledge, BARW models with this kind of reactions have not been studied yet. They form an interesting subject for further investigation.

The model of Cardy and Täuber has raised some interest recently since it has been found that fermionic and bosonic versions of the model are in different universality classes [19]. In the fermionic version only one particle per lattice site is allowed, which implies that particles of different species block each other. In the fermionic version of the model, it makes for instance a difference whether the two offsprings produced by the reaction (25) are placed to the same side or at opposite sides of the parent particle [19,20]. If, for in-

stance, they are placed at opposite sides the offsprings cannot annihilate through the reaction (23) because of the presence of the parent particle that blocks them. In the bosonic model, the two offspring can instead always recombine.

It is important to stress here that in the multispecies BARW model we constructed [Eqs. (21)–(22)] from a coarse-grained representation of the GCP there are no blocking effects. By the very construction of the model two domain walls approaching each other can always annihilate. Therefore, even if the model is clearly of fermionic nature its universality class, as found numerically, is that of the bosonic multispecies BARW.

## V. THE EFFECT OF BREAKING THE SYMMETRY

As a final point we consider the effect of breaking the permutation symmetry of the inactive states of the model. For  $n=2$  Hinrichsen [8] explicitly broke the  $Z_2$  symmetry by choosing  $\mu_1 \neq \mu_2$  in the reaction (2). As a result, he found the system to switch from PC to DP behavior, which was understood as PC being related to the presence of an exact  $Z_2$  symmetry.

For  $n=3$ , we now perform a similar symmetry breaking by considering the following two cases: (a)  $\mu_1/2 = \mu_2 = \mu_3$  and (b)  $2\mu_1 = \mu_2 = \mu_3$ . In both cases, the system has a  $Z_2$  symmetry due to the equivalence of the states  $0_2$  and  $0_3$ . The difference is that starting from a random configuration in the second case the system is more likely to reach the absorbing states  $(0_2, 0_2, 0_2, \dots)$  and  $(0_3, 0_3, 0_3, \dots)$  compared with  $(0_1, 0_1, 0_1, \dots)$ , while in the first case the reverse is true. We calculated the particle density  $\rho_L(\lambda, \mu_1, \mu_2, \mu_3)$  as before, using the boundary term (8). Depending on the phase in which the model is, the density will behave as  $\rho_L = \rho_0 + Ce^{-aL}$  (in the active region),  $\rho_L \sim L^{-\beta/\nu_{\perp}}$  (at criticality), or  $\rho_L \sim e^{-aL}$  (in the inactive phase). If we define  $\delta(L) = -\ln[\rho_{L+1}/\rho_L]/\ln[(L+1)/\ln(L-1)]$ , we expect  $\lim_{L \rightarrow \infty} \delta(L)$  to be zero in the active phase, to be  $\beta/\nu_{\perp}$  at critical points, and  $+\infty$  in the inactive phase. In Fig. 8 we plotted  $\delta(L)$  as a function of  $1/L$  for cases (a) and (b) with the choice  $\lambda=0.5$  and injection rate  $p'=1.5$ . In both cases, for small  $\mu$  one finds the typical scaling behavior of the active phase with  $\delta(L) \rightarrow 0$  just as for the case  $\mu_1 = \mu_2 = \mu_3$ . For large  $\mu_k$ , however, the situation differs from the symmetric model. For (a), we find  $\delta(L) \rightarrow +\infty$  for large  $\mu$ , i.e., one has a standard inactive phase with a particle density exponentially small in  $L$ . In case (b),  $\delta(L)$  becomes equal to one, implying that the inactive phase is itself critical with  $\beta/\nu_{\perp} = 1$ . In between the active and the inactive phase we have a critical point where  $\delta(L)$  is going to a distinct finite value. The critical point estimates of  $\delta(L)$  are marked by filled circles in Fig. 8. For case (a) the critical point is at  $\mu_1 \approx 0.64$ , while for (b) it is at  $\mu_1 \approx 0.42$ . The value of  $\beta/\nu_{\perp}$  agrees with that of DP and PC, respectively, as can be seen in Fig. 8 where the critical values of these universality classes are indicated with a dotted line.

This indicates that on breaking the symmetry of the inactive states, the remaining symmetry of the *dominant* rates  $\mu_i$  determines the critical behavior. In case (b),  $\mu_1 < \mu_2 = \mu_3$  the

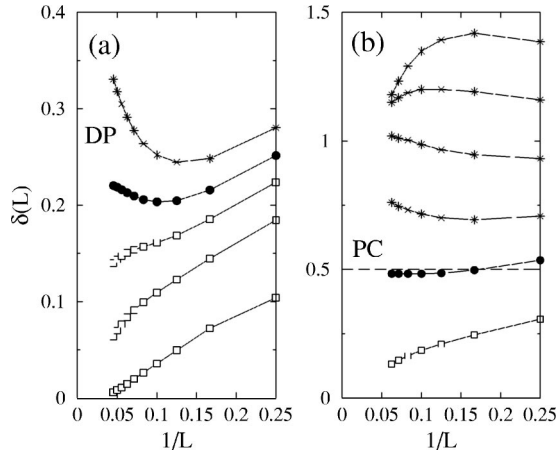


FIG. 8. Plot of  $\delta$  for the GCP with  $n=3$  and (a)  $\mu_1/2=\mu_2=\mu_3$ , (b)  $2\mu_1=\mu_2=\mu_3$ . Both cases were calculated with  $\lambda=0.5$  and  $p'=1.5$ . Symbols refer to curves calculated in the inactive phase (stars), at the critical point (filled circles) and in the active phase (empty squares). At criticality  $\delta(L)$  converges towards the values of  $\beta/\nu_\perp$  expected for DP (a) and PC (b), and indicated by horizontal dashed lines in the figure. Notice the two distinct behaviors of  $\delta$  in the inactive phase.

dominant rates still have a  $Z_2$  symmetry leading to the PC universality class, while in case (a)  $\mu_1 > \mu_2 = \mu_3$ , DP critical behavior is recovered.

## VI. CONCLUSIONS

In this paper, we studied a generalized contact process first introduced by Hinrichsen. The major part of our results were obtained by applying the DMRG to the model. With this technique we verified that for  $n=2$ , the critical line of the model is in the PC universality class, consistent with earlier results coming from simulations.

A first set of results was obtained for the case  $n=3$ , for which we found that the model is always active, except when  $\mu \rightarrow \infty$ , which corresponds to the critical line of the model. From our numerical work, we determined the critical exponents to be equal to  $z=2, \nu_\parallel=2$  and  $\beta=1$ . Using well-established scaling laws [21], other exponents can be determined from these three. For  $n=4$ , we found evidence that the phase diagram is the same, and that the critical exponent  $\beta$  also equals one. Secondly, using a fast-rate expansion that becomes exact for  $\mu \rightarrow \infty$ , we were able to argue that in that limit  $z=2$ . It can be hoped that by examining the model for  $\mu^{-1}$  small using perturbation techniques, it may be possible to determine also the exponents  $\beta$  and  $\nu_\parallel$  exactly. On the basis of these numerical and exact results, we conjectured that the universality class of the model is the same for all  $n \geq 3$ .

The exponent values that we found for  $n \geq 3$  coincide with those of the BARW model with more than one type of particles introduced by Cardy and Täuber [10]. We were able to give an heuristic argument that explains why the two models could be in the same universality class. It is interesting to remark that despite many attempts the number of universality classes found for phase transitions out of an adsorbing

phase, remains very limited. It could have been hoped *a priori* that for the generalized GCP studied here, new universality classes could appear for  $n > 2$ . In a sense our results show that this is true, but only in the least exciting way possible: the universality class does not depend on  $n$ , and moreover, the exponents take on rather trivial values. One could hope that by lowering the permutation symmetry to a  $Z_n$  symmetry, other universality classes could appear for  $n \geq 4$ . This could be done, e.g., by having the rates of the process (4) depend on  $|k-l| \bmod(n)$ . But since this would only make a difference for  $n \geq 4$ , it will probably be difficult to investigate such a model with the numerical techniques currently available.

We also verified that if one breaks the permutation symmetry of the model with  $n=3$ , one recovers a DP or PC universality, suggesting that it is the symmetry of the largest rates that determines the universality class.

Finally, we remark that the consistency of the DMRG results with those coming from simulation for  $n=2$ , or with the exactly determined value of  $z$  for  $n \geq 3$ , shows convincingly that the DMRG can be trusted as a powerful method in the study of (criticality in) non equilibrium systems.

## ACKNOWLEDGMENTS

J.H. and C.V. thank the IUAP, Belgium, for financial support. E.C. is grateful to INFM for financial support through PAIS 1999.

## APPENDIX

In this appendix, we will calculate explicitly,  $\lim_{r \rightarrow \infty} e^{-(H_0 + rH_1)t}$ , where  $r$  is one of the rates of the GCP. In Sec. III, it was shown that this reduces to the calculation of  $\tilde{H}_0 = T^*H_0T^*$ , the Hamilton that describes the effective dynamics. Since  $T^* = \lim_{t \rightarrow \infty} e^{-H_1t}$ , this is a projection of  $H_0$  on the ground states of  $H_1$ .

Let us denote the right ground states of  $H_1$  as  $|\psi_i\rangle$  and the left ones as  $\langle p_i|$ .

$$H_1|\psi_i\rangle = 0, \quad (\text{A1})$$

$$\langle p_i|H_1 = 0. \quad (\text{A2})$$

The physical meaning of  $|\psi_i\rangle$  is evident: they are the stationary states of  $H_1$ , any state  $|\psi\rangle$  will under the dynamics of  $H_1$  relax into one of these  $|\psi_i\rangle$ . The left ground states  $\langle p_i|$  can be interpreted as linear functionals giving the corresponding probabilities: any state  $|\psi\rangle$  will under the dynamics of  $H_1$  relax into the ground state  $|\psi_i\rangle$  with probability  $\langle p_i|\psi\rangle$  (where we assumed that  $\langle p_i|$  are normalized:  $\langle p_i|\psi_j\rangle = \delta_{ij}$ ). Using this notation, we can write the projection operator  $T^*$  as

$$T^* = \sum_i |\psi_i\rangle\langle p_i|. \quad (\text{A3})$$

Since, clearly,  $[\sum_i \langle p_i|]|\psi\rangle = 1$  for any (normalized) state  $|\psi\rangle$ , this projection conserves probability, meaning that when



$H_0$  is a stochastic operator, so is  $\tilde{H}_0$ . Furthermore, we can write the transition rates of the effective dynamics between state  $|\psi_i\rangle$  and  $|\psi_j\rangle$  as

$$\text{rate}(|\psi_i\rangle \rightarrow |\psi_j\rangle) = \langle p_j | (-H_0) | \psi_i \rangle. \quad (\text{A4})$$

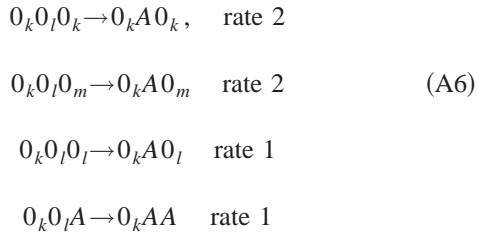
These matrix elements determine the effective dynamics, and we will now calculate them explicitly.

We first study the limit where the rate  $\mu$  of the processes  $A0_k, 0_k A \rightarrow 0_k 0_k$  goes to infinity. The Hamiltonian is of the form

$$H = H_0 + \mu H_1, \quad (\text{A5})$$

where  $H_0$  is the generator of the processes (1), (3), (4), and  $H_1$  is the generator of process (2) with the factor  $\mu$  brought out. In this case the ground states  $|\psi_i\rangle$  of  $H_1$  are all configurations containing no particles  $A$ . First, we note that the processes (1) and (3) can only act on configurations containing particles, so they cannot contribute to the rates (A4) of the effective dynamics, and we redefine  $H_0$  without them.

When we now project  $H_0$ , which contains only two-site interactions, onto the  $|\psi_i\rangle$ , the resulting operator will contain three-site interactions. It is therefore convenient to first rewrite  $H_0$  as a three-site operator. Since we only have reaction (4) left in  $H_0$ , this becomes ( $k \neq l \neq m$ )



(together with some reactions that are obtained by reflection). We finally notice that the last process of Eq. (A6) is again not relevant for the projection on  $|\psi_i\rangle$ , and determine the effective dynamics in the following diagram:

Reaction with rate	Projection with probability	Net rate
$0_k 0_l 0_k \xrightarrow{\text{rate } 2} 0_k A 0_k$	$\xrightarrow{1} 0_k 0_k 0_k$	rate $2 \cdot 1 = 2$
$0_k 0_l 0_m \xrightarrow{\text{rate } 2} 0_k A 0_m$	$\xrightarrow{1/2} 0_k 0_k 0_m$	rate $2 \cdot \frac{1}{2} = 1$
	$\xrightarrow{1/2} 0_k 0_m 0_m$	rate $2 \cdot \frac{1}{2} = 1$
$0_k 0_l 0_l \xrightarrow{\text{rate } 1} 0_k A 0_l$	$\xrightarrow{1/2} 0_k 0_k 0_l$	rate $1 \cdot \frac{1}{2} = \frac{1}{2}$
	$\xrightarrow{1/2} 0_k 0_l 0_l$	rate $1 \cdot \frac{1}{2} = \frac{1}{2}$

(A7)

which are the processes and their corresponding rates already given in Eqs. (18)–(20). Note that this calculation is exactly the same for  $\mu = \lambda \rightarrow \infty$ .

Next, we consider the limit  $\lambda \rightarrow \infty$ . In this case, we have

$$H = H_0 + \lambda H_1, \quad (\text{A8})$$

where  $H_0$  is the generator of the processes (2–4), and  $H_1$  is the generator of process (1) with the factor  $\lambda$  brought out. The ground states of  $H_1$  are now all configurations containing no particle pairs. In contrast with the previous case, all processes of  $H_0$  are now relevant for the projection on the ground states of  $H_1$ .

We will start with the case  $n = 1$ , where there is only one inactive state 0, and process (4) can *a priori* not take place. For process (3) we again use the three-site representation, while process (2) is so simple that we keep the two-site representation. We then get the following effective dynamics:

Reaction with rate . . .	Projection with probability . . .	Net rate
$A0 \xrightarrow{\text{rate } \mu} 00$	$\xrightarrow{1} 00$	rate $\mu \cdot 1 = \mu$
$A00 \xrightarrow{\text{rate } 1} AA0$	$\xrightarrow{1/2} A00$	rate $1 \cdot \frac{1}{2} = \frac{1}{2}$
	$\xrightarrow{1/2} 0A0$	rate $1 \cdot \frac{1}{2} = \frac{1}{2}$
$A0A \xrightarrow{\text{rate } 2} AAA$	$\xrightarrow{1/2} A0A$	rate $2 \cdot \frac{1}{2} = 1$
	$\xrightarrow{1/4} 0A0$	rate $2 \cdot \frac{1}{4} = \frac{1}{2}$
	$\xrightarrow{1/8} A00$	rate $2 \cdot \frac{1}{8} = \frac{1}{4}$
	$\xrightarrow{1/8} 00A$	rate $2 \cdot \frac{1}{8} = \frac{1}{4}$

(A9)

For  $\lambda \rightarrow \infty$  and  $n = 1$  we find the effective dynamics to contain only diffusion and destruction of particles. Because of the first reaction appearing in Eq. (A9), the decay of particles is exponentially fast, meaning that for any finite value of  $\mu$  this system is noncritical.

For the case  $n > 1$  also process (4) has to be taken into account. As a consequence, two different neighboring inactive domains remain active. For example,

$$0_k 0_l 0_l \rightarrow 0_k A 0_l \quad (\text{A10})$$

remains a process of the effective dynamics. One can easily construct the complete effective dynamics, but this does not lead to much further insight in the phase diagram. One can only conclude that because of the presence of the process (A10), it is in principle possible that both active and inactive phases are present.

- [1] J. Marro and R. Dickman, *Nonequilibrium Phase Transitions in Lattice Models* (Cambridge University Press, Cambridge, UK, 1996); H. Hinrichsen, *Adv. Phys.* **49**, 815 (2000).
- [2] T.E. Harris, *Ann. Prob.* **2**, 969 (1974).
- [3] H. Takayashu and A.Y. Tretyakov, *Phys. Rev. Lett.* **68**, 3060 (1992); I. Jensen, *Phys. Rev. E* **47**, 1 (1993).
- [4] E. Domany and W. Kinzel, *Phys. Rev. Lett.* **53**, 311 (1984).
- [5] I. Jensen, *Phys. Rev. Lett.* **70**, 1465 (1993).
- [6] P. Grassberger, F. Krause, and T. von der Twer, *J. Phys. A* **17**, L105 (1984).
- [7] H. Park and H. Park, *Physica A* **26**, 3921 (1993).
- [8] H. Hinrichsen, *Phys. Rev. E* **55**, 219 (1997).
- [9] *Density Matrix Renormalization: A New Numerical Method in Physics*, Lecture Notes in Physics, edited by I. Peschel, X. Wang, M. Kaulke, and K. Hallberg (Springer, New York, 1999).
- [10] J. Cardy and U. Täuber, *Phys. Rev. Lett.* **77**, 4780 (1996); *J. Stat. Phys.* **90**, 1 (1998).
- [11] M. Kaulke and I. Peschel, *Eur. Phys. J. B* **5**, 727 (1998); E. Carlon, M. Henkel, and U. Schollwöck, *ibid.* **12**, 99 (1999).
- [12] E. Carlon, M. Henkel, and U. Schollwöck, *Phys. Rev. E* **63**, 036101 (2001).
- [13] F.C. Alcaraz, M. Droz, M. Henkel, and V. Rittenberg, *Ann. Phys. (N.Y.)* **230**, 250 (1994).
- [14] G. M. Schütz, in *Phase Transitions and Critical Phenomena*, edited by C. Domb and J. L. Lebowitz (Academic, London, 2000) Vol. 19.
- [15] The transformation (7) was also implemented in Ref. [12].
- [16] It should be noted that rigorously for the calculation of the exponent  $z$  one should first extrapolate the value of  $\mu_{\max}(L)$  to the thermodynamic limit  $L \rightarrow \infty$  to obtain an estimate of the critical value  $\mu_c$ . Then perform another extrapolation  $Y_L(\mu_c) \rightarrow -z$ . However, in the present model, both numerical procedures give the same extrapolated value for  $z$ . For a more detailed discussion on this point, see Appendix B of Ref. [12]. Notice also that since the maxima of  $Y_L(\lambda, \mu)$  are not so pronounced, one can locate accurately their ordinates, while their abscissas are somewhat less accurate. This is the reason why extrapolated values of  $z$  are more accurate than the location of the critical point itself.
- [17] M. Droz, J. Kamphorst Leal da Silva, A. Malaspina, and J. Yeomans, *J. Phys. A* **19**, 2671 (1986).
- [18] B. Derrida, V. Hakim, and V. Pasquier, *J. Stat. Phys.* **85**, 763 (1996).
- [19] S. Kwon, J. Lee, and H. Park, *Phys. Rev. Lett.* **85**, 1682 (2000).
- [20] G. Odor, *Phys. Rev. E* **63**, 021 113 (2000).
- [21] P. Grassberger and A. de la Torre, *Ann. Phys. (N.Y.)* **122**, 373 (1979).